Overall viscoplastic behavior of non-irradiated porous nuclear ceramics

Yann Monerie, Jean-Marie Gatt

Overall viscoplastic behavior of non-irradiated porous nuclear ceramics

Yann Monerie, Jean-Marie Gatt

CE Cadarache CEA/DEN/DEC, 13108 Saint-Paul lez Durance, France

This paper deals with the overall behavior of nonlinear viscous and porous nuclear ceramics. Bi-viscous isotropic por-ous materials are considered: the matrix is subjected to two power-law viscosities with different exponents related to two stationary temperature-activated creeping mechanisms (scattering-creep and dislocation-creep), and this matrix contains a low porosity volume fraction. The overall behavior of these types of composite materials is obtained with the help of quadratic strain-rate potentials combined with experimental-based coupling function depending on stress and temperature. For each creeping mechanism, the hollow sphere model of [Michel, J.-C., Suquet, P., 1992. The constitutive law of non-linear viscous and porous materials. Journal of the Mechanics and Physics of Solids 40, 783–812] is used. Mechanical parameters of the resulting model are identified and validated in the particular case of non-irradiated uranium dioxide nuclear ceramics. This model predicts, under pure thermo-mechanical loading, a variation of the material volume and a variation of the porosity volume fraction (the so-called densification or swelling).

Keywords: Overall behavior; Porous materials; Nonlinear viscosity; Nuclear ceramics

1. Introduction

This paper examines the overall nonlinear behavior of nuclear ceramics. In particular, our attention focuses on an elastoviscoplastic mechanical model for the stationary creep of porous non-irradiated UO_2 nuclear fuel.

The main mechanism of interest is the change of cavities volume under mechanical loading. These cavities are due to fabrication process and could be considered as voids (porosities without internal pressure). This change of porosity volume fraction plays a determinant role in the creep of crystalline materials at high temperature.

A viscoplastic model is proposed which depends on the porosity volume fraction and is coupled with the evolution of this porosity under mechanical loading. This model is obtained with the help of micromechanics. The macroscopic strain-rate potential is deduced from microstructure and from microscopic strain-rate potentials corresponding to each nonlinear viscous behaviors of the UO_2 matrix: scattering-creep and dislocation-creep. For each creeping

E-mail address: yann.monerie@irsn.fr (Y. Monerie).
Corresponding author. Present address: CE Cadarache IRSN/DPAM, BP3-13115 Saint-Paul lez Durance Cedex, France. Tel.: +33 442199617; fax: +33 442199166.

mechanism at the microscale, a quadratic macroscopic strain-rate potential denoted by Ψ_i (for $i = 1, 2$) is chosen (each creeping mechanism is considered as an independent phase). Both potentials are coupled using a function denoted by θ. The final macroscopic strain-rate potential has the following form:

$$\Psi = (1 - \theta)\Psi_1 + \theta\Psi_2, \tag{1}$$

where the coupling function θ depends on the temperature and on the stress (scattering-creep acts for low temperatures and small stresses, dislocation-creep acts for high temperatures and high stresses).

In the first part, after the presentation of the models corresponding to each strain-rate potential Ψ_i $(i = 1, 2)$, the coupling function is determined and the numerical implementation of the final model is given.

In the second part, the mechanical parameters of the model are identified on uniaxial compressive creeping tests and validated on uniaxial compressive tests at prescribed strain-rate for various temperatures and microstructrures (various porosity volume fractions and various grain sizes).

2. Constitutive law of nonlinear viscous and porous non-irradiated UO_2 material

2.1. Micro–macro approach

2.1.1. Methodology

At high temperature (typically $T \geqslant 1000$ °C), the evolution of porosity volume fraction has a significant role in the creep of ceramics. A stationary creep model for UO_2 material has to take into account the influence of the evolution of porosity in a strong way. Concerning the UO_2 nuclear fuel this evolution of initial porosity has three main causes: accumulation of vacancies at the grain boundaries, deformation of the matrix by mechanical loading, and evolution of bubbles of fission products for irradiated nuclear fuel. This paper focuses on the second point: evolution of porosity volume fraction by mechanical effects.

Using a micromechanical approach, a model for the elastoviscoplastic behavior of the porous ceramics is proposed. This model is devoted to the UO_2 nuclear fuel considering porosities as voids without internal pressure (the atmospheric pressure corresponding to the compaction process is neglected). The overall behavior of this material is governed by a strain-rate potential deduced from the microstruture and from the microscopic potentials related to nonlinear viscosities identified at this microscale. The proposed model is written in the context of continuum thermodynamics.

The considered microstructure and the micromechanical parameters are presented in the following section.

2.1.2. Representative Volume Element (RVE), microstructure and macroscopic variables

The so-called homogenization methods do not lead to the exact behavior of a multiphase material but allow to establish convenient approximations such as bounds or estimates (see Milton (2002) for a recent overview). In most cases, effective lower and upper bounds are very far apart because of the lack of information on the microstructure or because it is not possible to model all microstructural information. In the particular case of porous materials, the difference between lower and upper bounds is maximal, and estimates are used to approximate the effective behavior of porous materials (with respect to the bounds).

The UO_2 nuclear fuel is fabricated by compaction process. It could be considered as a porous ceramic matrix which includes porosities randomly distributed in space and shape. In order to use homogenization approaches a Representative Volume Element (RVE), denoted by $\mathscr{V}$, is chosen. This volume is large enough to consider the UO_2 nuclear fuel as an isotropic matrix including porosities only characterized by their volume fraction (see definition of f in a following paragraph). It should be noticed that the assumptions of a continuous matrix requires perfect grain boundaries (no sliding) and suggests that the material properties could be measured independently of grain orientations.

Macroscopic variables using volume averages should be defined carefully in the presence of cavities (see e.g., Zaoui, 2001, and references therein). $\mathscr{P}$ represents the domain occupied by porosities, $|x|$ the volume of any part x of $\mathbb{R}^3$, σ the microscopic Cauchy stress, and $\dot{\varepsilon}$ the microscopic Eulerian strain-rate in $\mathscr{V} - \mathscr{P}$. The macroscopic stresses Σ and the macroscopic strain rates $\dot{E}$ are defined as volume averages of the corresponding microscopic quantities in the following generalized sense (Michel and Suquet, 1992):

$$\begin{aligned} \Sigma &= \langle\sigma\rangle = \frac{1}{|\mathscr{V}|}\int_{\mathscr{V}-\mathscr{P}} \sigma \,\mathrm{d}x \quad \text{and} \\ \dot{E} &= \frac{1}{|\mathscr{V}|}\int_{\partial\mathscr{V}} \dot{u}\otimes_S v \,\mathrm{d}s, \end{aligned} \tag{2}$$

where $\partial\mathscr{V}$ denotes the outer boundary of the RVE, v the outer unit vector on $\partial\mathscr{V}$, u the displacement field, and $a\otimes_S b = \frac{1}{2}(a_i b_j + a_j b_i)$ for any vector a and b.

The strain-rate potential of the nonlinear viscous UO_2 matrix is taken as Newtonian viscous potential:

$$\psi(\sigma) = \frac{\sigma_0 \dot{\varepsilon}_0}{n+1}\left(\frac{\sigma_{eq}}{\sigma_0}\right)^{n+1}, \tag{3}$$

where σ_{eq} represents the second invariant of the stress $\sigma_{eq} = \sqrt{\frac{3}{2}\sigma^D : \sigma^D}$ (σ^D being the stress deviator), n represents the so-called Norton exponent ($1 \leqslant n \leqslant +\infty$), and σ_0 and $\dot{\varepsilon}_0$ represent material constants. The microscopic behavior associated to this type of potential is given by

$$\dot{\varepsilon} = \frac{\partial\psi}{\partial\sigma}(\sigma) = \dot{\varepsilon}_0\left(\frac{\sigma_{eq}}{\sigma_0}\right)^{n-1}\frac{3}{2}\frac{\sigma^D}{\sigma_0}. \tag{4}$$

The extreme cases of a linear Newtonian viscosity and of a rigid-plastic behavior correspond respectively to the cases $n = 1$ and $n = +\infty$. As it will be shown in a next section, physical considerations lead to consider two (4)-type strain-rates for the UO_2 matrix behavior.

A description of the UO_2 fuel material could be found in Nogita and Une (1995). From this work, the only retained parameter for describing its microstructure is the porosity volume fraction defined as

$$f = \frac{|\mathscr{P}|}{|\mathscr{V}|}. \tag{5}$$

Due to the incompressibility of the UO_2 matrix (see Eq. (4)), the porosity growth rate is governed by the macroscopic mass balance equation obtained using (5) and (2):

$$\dot{f} = (1-f)\mathrm{Tr}(\dot{\mathscr{E}}). \tag{6}$$

2.1.3. Macroscopic potential of nonlinear viscous and porous materials

In this section, the general quadratic form of the macroscopic strain-rate potential corresponding to a nonlinear viscous matrix including porosities is presented. The specific dependence of the model parameters on the porosity volume fraction is explained through a short bibliographic overview.

For a given viscous mechanism, the macroscopic strain-rate potential respects the following average relation:

$$\Psi(\Sigma) = \langle\psi(\sigma)\rangle. \tag{7}$$

As mentioned above, the UO_2 fuel microstructure is characterized by randomly distributed porosities in space and size. The UO_2 fuel material could be then considered as isotropic at the macroscale and a scalar parameter (the porosity volume fraction f) is sufficient for a convenient description of the microstructure. The macroscopic potential Ψ is thus a function of f and of the three invariants of the macroscopic stress Σ, namely Σ_m (the hydrostatic stress $\Sigma_m = \frac{1}{3}\mathrm{Tr}(\Sigma)$), Σ_{eq} and $\det(\Sigma)$. In what follows, the classical assumption that Ψ does not depend on $\det(\Sigma)$ is made:

$$\Psi = \Psi(\Sigma, f) = \Psi(\Sigma_m, \Sigma_{eq}, f). \tag{8}$$

This last assumption was checked by Duva and Hutchinson (1984) for nonlinear materials including low porosity volume fraction (typically $f \leqslant 10\%$). In addition, relations (3) and (7) imply that Ψ, as the local strain-rate potential, is a convex function of Σ positively homogeneous of degree $n+1$:

$$\Psi(\lambda\Sigma, f) = |\lambda|^{n+1}\Psi(\Sigma, f) \quad \forall\lambda \in \mathbb{R}. \tag{9}$$

Using properties (8) and (9), Ψ could be written in the following form:

$$\Psi(\Sigma, f) = \frac{\sigma_0\dot{\varepsilon}_0}{n+1}\left(A(f)\left(\frac{3}{2}\frac{\Sigma_m}{\sigma_0}\right)^2 + B(f)\left(\frac{\Sigma_{eq}}{\sigma_0}\right)^2\right)^{\frac{n+1}{2}}. \tag{10}$$

This quadratic form was initially proposed by Berg (1970) and by other authors in various contexts (Michel, 1994; Olevsky and Skorohod, 1988; Shima and Oyane, 1976; Sofronis and McMeeking, 1992). This form meets those obtained by Cocks (1989) with the help of variational estimate, the form of nonlinear bounds of Suquet (1992) and Ponte Castañeda (1991), and the form obtained by Talbot and Willis (1992) using new variational principles.

The complete writting of the model is given with parameters $A(f)$ and $B(f)$. In the next section, the choice for these parameters and a review of existing models are presented.

2.1.4. Parameters of the quadratic strain-rate potential

Without porosity, the macroscopic behavior is identical to the local behavior:

$$\Psi = \psi, \tag{11}$$

which leads readily to the following conditions on parameters $A(f)$ and $B(f)$:

$$A(f) \overset{f\to 0}{\to} 0 \quad \text{and} \quad B(f) \overset{f\to 0}{\to} 1. \tag{12}$$

The variational estimate of Cocks (1989) leads to the specific choice:

$$\begin{aligned} A(f) &= \frac{f}{f+1}\frac{2n}{n+1}(1-f)^{\frac{-2n}{n+1}} \quad \text{and} \\ B(f) &= \left(1+\frac{2}{3}f\right)(1-f)^{\frac{-2n}{n+1}}, \end{aligned} \tag{13}$$

where $B(f)$ is not exactly deduced from the direct variational estimate but corrected to closer meet some analytical solutions.

The rigorous lower nonlinear bound, initially introduced by Ponte Castañeda and Willis (1988), redefined by Ponte Castañeda (1991) and Talbot and Willis (1992) with help of new variational principles, and deduced again by Michel and Suquet (1992) with simpler arguments, corresponds to

$$\begin{aligned} A(f) &= f(1-f)^{\frac{-2n}{n+1}} \quad \text{and} \\ B(f) &= \left(1+\frac{2}{3}f\right)(1-f)^{\frac{-2n}{n+1}}. \end{aligned} \tag{14}$$

We emphazise that the parameter $B(f)$ of this rigorous lower bound meets exactly the expression proposed by Cocks (1989).

As underlined by Michel and Suquet (1992), none of these models gives the exact solution of a hollow sphere made of nonlinear incompressible viscous material under hydrostatic loading. This exact solution, first given by Budiansky et al. (1982), reads

$$A(f) = \left(n\left(f^{\frac{-1}{n}}-1\right)\right)^{\frac{-2n}{n+1}}. \tag{15}$$

The model (10) corresponding to this parameter is exact on the simplest elementary porous cell: the hollow sphere.

The self-consistent scheme proposed by Michel and Suquet (1992) gives the ratio $D = A(f)/B(f)$ solving the equation:

$$\begin{aligned} \widehat{C}(n^2)\log(f) = -\widehat{C}(n)\log(\widehat{C}(n)) + \frac{n+1}{2n^2D}\log(\widehat{C}(1)) \\ + \frac{n-1}{n\sqrt{D}}\left(\arctan(\sqrt{D}) - \frac{\pi}{2}\right), \end{aligned} \tag{16}$$

where

$$\widehat{C}(x) = 1 + \frac{1}{xD} \quad \forall x \in \mathbb{R}. \tag{17}$$

Assuming that the strain-rate deviator tensor could be correctly approximated by an averaged norm in the stress potential (i.e. the conjugate of the strain-rate potential in (3)), Michel (1994) proposes a complete self-consistent estimate, which gives the parameters $A(f)$ and $B(f)$ solving the set of equations (16) and (17) and the following equation:

$$\begin{aligned} B(f) &= \frac{1}{\tilde{\mu}}(1-f)^{\frac{-2n}{n+1}}, \quad \text{where} \\ \tilde{\mu} &= \frac{1 - f/\bar{f}(n)}{(1-f)(1-f/3^n)\left(1-\frac{n-1}{2n}f\right)} \end{aligned} \tag{18}$$

with values of $\bar{f}(n)$ given in Table 1 for spherical porosities.

The model used in this paper is the so-called "hollow sphere model" (Michel and Suquet, 1992) retaining for the parameter $A(f)$ the exact solution of an hollow sphere made of nonlinear incompressible viscous material under hydrostatic loading (15). This one predicts a porosity growth rate higher than the rate corresponding to the lower bound (14) and lower than the rate corresponding to the self-consistent estimate of Michel (1994) (see Fig. 1), and for parameter $B(f)$ the lower bound (14), which is equivalent for many presented models. The retained model is at least defined by the following parameters:

$$\begin{aligned} A(f) &= \left(n\left(f^{\frac{-1}{n}}-1\right)\right)^{\frac{-2n}{n+1}} \quad \text{and} \\ B(f) &= \left(1+\frac{2}{3}f\right)(1-f)^{\frac{-2n}{n+1}}. \end{aligned} \tag{19}$$

Table 1
Numerical values of $\bar{f}$ for various Norton exponents and spherical porosities (from Michel, 1994)

n	1	3	5	10	∞
$\bar{f}(n)$	0.5	0.448	0.430	0.414	0.392

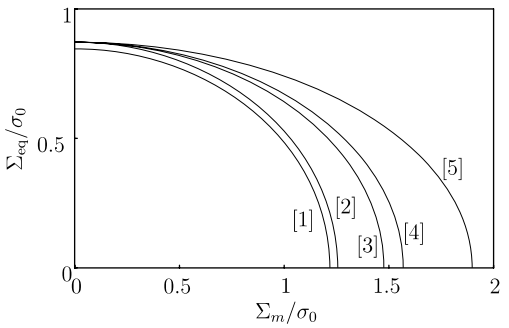

Fig. 1. Equipotential surfaces $\Psi = (1-f)\sigma_0\dot{\varepsilon}_0/(n+1)$ for $f = 0.1$ and $n = 10$: [1] complete self-consistent scheme of Michel (1994), [2] self-consistent scheme of Michel and Suquet (1992), [3] model of Cocks (1989), [4] hollow sphere model, [5] lower nonlinear bound of Ponte Castañeda (1991).

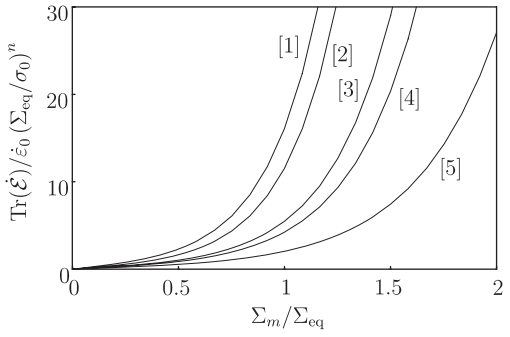

Fig. 2. Evolution of the macroscopic normalized dilatation rate versus triaxiality rate for $f = 0.1$ and $n = 10$: [1] complete self-consistent scheme of Michel (1994), [2] self-consistent scheme of Michel and Suquet (1992), [3] model of Cocks (1989), [4] hollow sphere model, [5] lower nonlinear bound of Ponte Castañeda (1991).

Following Michel (1994), this model is compared in Figs. 1 and 2 to others presented models. In Fig. 1, equipotential surfaces $\Psi = (1-f)\sigma_0\dot{\varepsilon}_0/(n+1)$ are plotted for non-negative triaxiality ratio $\Sigma_{\mathrm{m}}/\Sigma_{\mathrm{eq}}$, $f = 0.1$ and $n = 10$. In Fig. 2, corresponding evolutions of the macroscopic normalized dilatation rate are given as a function of triaxiality.

The hollow sphere model defined by (10) and (19) corresponds to a power law matrix including porosities described only by their volume fraction. According to Figs. 1 and 2, this model predicts an intermediate porosity growth rate between self-consistent schemes (some other self-consistent estimates, like those of Leblond and Perrin (1992), lead to equivalent porosity growth rates versus triaxiality than those of Michel (1994) and Michel and Suquet (1992)) and the rigorous nonlinear lower bound of Ponte Castañeda (1991). This model is coupled to an evolution of the microstructure by (6). It is dedicated to the stationary creep of nonlinear and porous materials and in particular to high temperature porous ceramics like UO_2 nuclear fuel. In the next section, we focus on the two elementary viscous mechanisms acting in the UO_2 matrix.

2.2. Taking into account different stationary creeps and elasticity

In this section, the generic model (10) and (19) is particularized to the UO_2 nuclear fuel.

For strain rates ranging between about 1.1×10^{-5} s^{-1} and 1.1×10^{-3} s^{-1}, and temperatures ranging between 870 K and 1970 K, compressive tests performed on stoichiometric, sintered polycristalline UO_2 show that two different creeping mechanisms have to be considered at the microscale (Guerin, 1975; Millet and Piconi, 1983): scattering-creep and dislocation-creep. Each of these mechanisms depends on temperature, stress and grain size. A convenient description of these mechanisms is obtained with a power-law involving an Arrhenius-like temperature influence, and a power-law dependence to the grain size d ($i = 1, 2$):

$$\dot{\varepsilon}_{0_i} = \dot{\tilde{\varepsilon}}_{0_i} d^{m_i} \mathrm{e}^{-\frac{Q_i}{RT}}, \tag{20}$$

where $\dot{\tilde{\varepsilon}}_{0_i}$ represents a material constant, m_i represents an exponent, Q_i represents an activation energy for the ith mechanism, and R the perfect gas constant. The corresponding macroscopic potentials have the form obtained in the above section ($i = 1, 2$):

$$\begin{aligned}\Psi_i(\Sigma, f) &= \Psi_i(\Sigma_{\mathrm{m}}, \Sigma_{\mathrm{eq}}, f, d, T)\\ &= \frac{\sigma_{0_i}\dot{\tilde{\varepsilon}}_{0_i}}{n_i+1}\quad A(f)\left(\frac{3}{2}\frac{\Sigma_{\mathrm{m}}}{\sigma_{0_i}}\right)^2\\ &\quad + B(f)\left(\frac{\Sigma_{\mathrm{eq}}}{\sigma_{0_i}}\right)^2\Bigg)^{\frac{n_i+1}{2}} d^{m_i}\mathrm{e}^{-\frac{Q_i}{RT}},\end{aligned} \tag{21}$$

where σ_{0_i} represent constants and n_i represent the Norton exponents for each mechanism.

In a theoretical way, the existence at the microscale of two separate dissipative mechanisms should lead at the macroscale to a long-time memory effect added to the separate effects of each mechanism (Suquet, 1982). This effect is not directly taken into account here, but a macroscopic model where the separate effects of each mechanism are combined through physical arguments is proposed.

As observed (for example by Guerin, 1975), the scattering-creep acts for small stresses and at low temperatures, and the dislocation-creep acts for large stresses and at high temperatures. A coupling of these two mechanisms is proposed (already dependent on temperature within the term $\mathrm{e}^{-\frac{Q_i}{RT}}$) by a function depending on the macroscopic stress and on the temperature.

With the retained coupling the macroscopic strain-rate potential reads:

$$\Psi = (1-\theta)\Psi_1 + \theta\Psi_2. \tag{22}$$

The coupling function θ is equal to zero when only scattering-creep acts, and equal to 1 when only dislocation-creep acts. The chosen coupling function is

$$\theta(T,\Sigma)=\frac{1}{2}\left(1+\tanh\left(\frac{T-\bar{T}(\sqrt{\Sigma:\Sigma})}{h}\right)\right), \tag{23}$$

where h represents a constant and $\bar{T}(\Sigma_{\text{eq}})$ a temperature of transition which depends on the macroscopic equivalent von Mises stress.

The temperature of transition could be obtained directly from experimental measurements as the deformation-mechanisms maps of Frost and Ashby (1982). According to these maps, a convenient power law could be retained for $\bar{T}$:

$$\bar{T}(x)=\omega x^{q} \quad \forall x>0. \tag{24}$$

Using the following relations giving respectively the macroscopic viscoplastic strain-rates corresponding to each creeping mechanism ($i=1,2$):

$$\dot{\mathscr{E}}_{\text{vp}_i}=\partial\Psi_i, \tag{25}$$

the final model reads

$$\dot{\mathscr{E}}_{\text{vp}}=(1-\theta)\dot{\mathscr{E}}_{\text{vp}_1}+\theta\dot{\mathscr{E}}_{\text{vp}_2}+(\Psi_2-\Psi_1)\frac{\partial\theta}{\partial\Sigma}, \tag{26}$$

where, for $i=1,2$ ($\mathbb{I}$ denotes the 3×3 identity matrix):

$$\dot{\mathscr{E}}_{\text{vp}_i}=\frac{\dot{\bar{\varepsilon}}_{0_i}}{2}\quad A_i(f)\left(\frac{3}{2}\frac{\Sigma_{\text{m}}}{\sigma_{0_i}}\right)^2+B_i(f)\left(\frac{\Sigma_{\text{eq}}}{\sigma_{0_i}}\right)^2\Bigg)^{\frac{n_i-1}{2}} \times\left(A_i(f)\left(\frac{3}{2}\frac{\Sigma_{\text{m}}}{\sigma_{0_i}}\right)\mathbb{I}+3B_i(f)\left(\frac{\Sigma^{D}}{\sigma_{0_i}}\right)\right)d^{m_i}\mathrm{e}^{-\frac{Q_i}{RT}}. \tag{27}$$

It should be underlined that the coupling from two microscopic creeps (22) leads to three macroscopic creeps (see (26)) as experimentally observed by (Sladkoff et al., 2000). However, it should be noticed that this class of coupling does not allow to couply with the homogeneity rule (9).

This macroscopic viscoplastic model is completed by taking into account the elastic behavior, assuming after Leclercq (1998) the additivity of macroscopic strains (assumption of small strains for nuclear pellet):

$$\Sigma=C^{\text{hom}\,-1}:(\mathscr{E}-\mathscr{E}_{\text{vp}}), \tag{28}$$

where C^{hom} represents the effective elastic tensor of the porous UO_2 nuclear fuel. This effective elastic tensor is supposed to be isotropic. This was checked by three-dimensional numerical simulations involving spherical and ellipsoidal porosities (Gatt et al., 2005), that the values of C^{hom} given by Martin (1989) based on experimental reviews are convenient estimates for numerous elaborating process of the UO_2 nuclear fuel. Without additional information on the particular microstructure of the studied UO_2 nuclear fuel, the following overall Young E^{hom} and bulk μ^{hom} moduli are retained:

$$E^{\text{hom}}(f,T)=(226930-15.339T-9.597\times10^{-3}T^2)\times(1-2.5f), \tag{29}$$

$$\mu^{\text{hom}}(f,T)=(85830-5.157T-3.747\times10^{-3}T^2)\times(1-2.25f), \tag{30}$$

where E^{hom} and μ^{hom} are in MPa and temperature T in Kelvin.

It should be emphasized that the overall elastoviscoplastic behavior defined in (28) does not account for the evolution of porosity (6) based on the assumption of the incompressibility of the matrix. Following Chaboche et al. (2001), the classical approximated mass balance is used:

$$\dot{f}\simeq(1-f)\mathrm{Tr}(\dot{\mathscr{E}}_{\text{vp}}). \tag{31}$$

This model is obviously rigorous for pure creep conditions, but approximated for other loadings.

2.3. Numerical implementation

The final model is constituted by a system of differential equations. The constitutive law (26) is solved by a Θ-method ($\Theta=\frac{1}{2}$) and the equation of evolution of the microstructure (31) is solved using an implicit Euler scheme. The coupled system is solved with the help of a fixed point method checking that the partial derivative of C^{hom} with respect to T and f are neglectible in comparison to the other terms. The convergence of this fixed point method is ensured by a criterion on the unknown global vector $Y=\{\dot{\mathscr{E}}_{\text{vp}},\Sigma,f\}$:

$$\|Y^{k+1}-Y^{k}\|<\alpha\|Y^{k}\|, \tag{32}$$

where Y^k denotes the value of Y at iteration k and the parameter α is taken equal to 10^{-5}. These solving methods and associated algorithms are implemented on MATHEMATICA®.

In the next section, the mechanical parameters of the proposed model are identified and validated on compressive tests.

3. Identification of mechanical parameters and validation of the model

Some mechanical parameters of the model are taken equal to their theoretical values corresponding

to physical mechanisms (e.g., exponents of each creeping mechanism), and others mechanical parameters are identified on compressive creeping tests. The model is validated on compressive tests at various prescribed macroscopic strain-rates and various temperatures.

3.1. Identification

As already mentioned, the evolution of the transition temperature $\bar{T}$ with the macroscopic stress is estimated using the diagrams of Frost and Ashby (1982). A convenient approximate of this evolution is given by (24) with parameters ω and q given in Table 3.

The other parameters of the model are identified on the experimental data base presented in (Sladkoff et al., 2000). The concerned experiments are compressive tests on non-irradiated and non-doped UO_2 pellet. The range of identification is given in Table 2, both for external loadings and microstructural parameters. The identified mechanical parameters (for each creeping mechanism: energies of activation Q_i, Norton exponents n_i, exponents on grain size m_i and multiplicative constants $\dot{\bar{\varepsilon}}_{0_i}/(\sigma_{0_i})^{n_i}, i = 1, 2$) and the parameter h are given in Table 3. The agreement between experimental data and numerical simulations are plotted in Fig. 3.

Table 2
Identification range of mechanical parameters listed in Table 3

External loading	
$20\ \text{MPa} \leqslant \Sigma_{11} \leqslant 100\ \text{MPa}$	$1570\ \text{K} \leqslant T \leqslant 1950\ \text{K}$
Microstructural parameters	
$0.81\% \leqslant f \leqslant 7\%$	$4.5\ \mu\text{m} \leqslant d \leqslant 26\ \mu\text{m}$

Table 3
Mechanical parameters of the model

Scattering-creep			
n_1	m_1	Q_1	$\dot{\bar{\varepsilon}}_{0_1}/(\sigma_{0_1})^{n_1}$
1	-2	$377 \times 10^3\ \text{J mol}^{-1}$	$7.57 \times 10^{-14}\ \text{s}^{-1}\ \text{N}^{-n_1}\ \text{m}^{2n_1-m_1}$
Dislocation-creep			
n_2	m_2	Q_2	$\dot{\bar{\varepsilon}}_{0_2}/(\sigma_{0_2})^{n_2}$
8	2	$462 \times 10^3\ \text{J mol}^{-1}$	$2.54 \times 10^{-44}\ \text{s}^{-1}\ \text{N}^{-n_2}\ \text{m}^{2n_2-m_2}$
Temperature of transition			
h		ω	q
600 K		$47350.4\ \text{K N}^{-q}\ \text{m}^{2q}$	-0.189

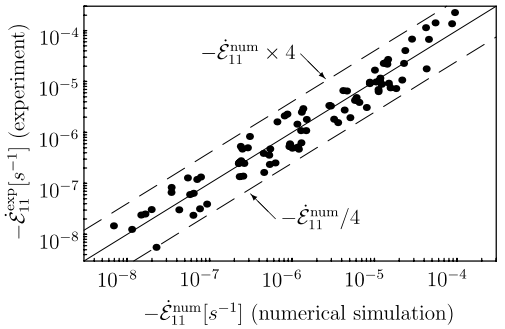

Fig. 3. Macroscopic uniaxial strain-rate: comparison between numerical simulations and experimental data during creeping compressive tests.

3.2. Comments on the identified parameters of the model

The following comments on the identified parameters hold:

(1) About the coupling function: the parameters of the function θ are identified apart from others parameters (on the experimental data base of Frost and Ashby (1982)). For this function, only the parameter h was considered as a fitting parameter.
(2) About the scattering-creep mechanism: since this mechanism seems to be well understood at the microscale, we retain for the identification the most classical values for the parameters n_1, Q_1 and m_1. Most of the authors agrees with the values:
- $n_1 = 1$ (Bohaboy et al., 1969),
- $Q_1 = 377 \times 10^3\ \text{J mol}^{-1}$ which is the theoretical values of grain boundary diffusion energy (Bohaboy et al., 1969; Knorr et al., 1989),
- $m_1 = -2$ for $4\ \mu\text{m} \leqslant d \leqslant 40\ \mu\text{m}$ (Bohaboy et al., 1969; Armstrong and Irvine, 1963).

It should be noticed that recent works of Dherbey et al. (2002) proposed a larger value of n_1 ($n_1 = 2.6$), a value of Q_1 between $359 \times 10^3\ \text{J mol}^{-1}$ for a power law (σ^{n_1}) and $380 \times 10^3\ \text{J mol}^{-1}$ for an exponential law (e^{σ}), and a value of m_1 about -1.3. The review by Wang (2000) proposed $Q_1 = 368 \times 10^3\ \text{J mol}^{-1}$, $n_1 = 1$ and $m_1 \in [-2, -3]$. This range for m_1 is also obtained by Chung and Davies (1979) and confirmed by Knorr et al. (1989) ($m_1 \simeq -2.67$ for $2\ \mu\text{m} \leqslant d \leqslant 55\ \mu\text{m}$) and Burton et al. (1973) ($m_1 \simeq -3$). Concerning

this first creep mechanism, the mechanical parameters of the present model agree well with usual values of scattering-creep elementary mechanisms.

(3) About the dislocation-creep mechanism: the obtained value for the Norton exponent $n_2 = 8$ has to be considered as an upper value of those involved in the literature. Javed (1975) proposes $n_2 = 4.3$, Bohaboy et al. (1969) retain $n_2 = 4.5$ for $1723\ \mathrm{K} \leqslant T \leqslant 2023\ \mathrm{K}$, Dherbey et al. (2002) find $n_2 = 6.2$ and Guerin (1975) suggests $4.5 \leqslant n_2 \leqslant 17$. Concerning the parameter Q_2, the identified value ($Q_2 = 462 \times 10^3\ \mathrm{J\ mol^{-1}}$) lies between the theoretical uranium self-diffusion energy $Q_2 = 544 \times 10^3\ \mathrm{J\ mol^{-1}}$ (Knorr et al., 1989) or the value retained by Bohaboy et al. (1969) ($Q_2 = 552 \times 10^3\ \mathrm{J\ mol^{-1}}$) or by Dherbey et al. (2002) ($Q_2 = 524 \times 10^3\ \mathrm{J\ mol^{-1}}$), and the value proposed by Javed (1975) ($Q_2 = 338 \times 10^3\ \mathrm{J\ mol^{-1}}$). The identified value in this paper is in agreement with Guerin (1975). Concerning the identified grain size exponent $m_2 = 2$, it is often considered that this creeping mechanism has no grain size-dependence (Bohaboy et al., 1969; Seltzer et al., 1971; Wang and Nieh, 1996), but the works of Burton et al. (1973) confirm that $m_2 > 0$. The Norton exponent $n_2 = 8$ and the grain size exponent $m_2 = 2$ have to be considered as significant results of this work.

3.3. Validation

3.3.1. Compressive tests

The results plotted in Figs. 4 and 5 show the ability of the proposed model to predict the behavior of the UO_2 pellet during various experiments. For example, this model predicts with a good agreement the ultimate steady stress, denoted by $\bar{\Sigma}$, during a compressive test at prescribed strain-rate for various temperatures and various initial microstructures (porosity volume fraction and grain size).

On Fig. 6, a severe comparison is made between the measured evolution of the macroscopic strain during compressive creeping tests for various temperatures and applied stress and the behavior predicted by the present model. These experiments concern initial microstructures defined by a grain size of 12.5 μm and a porosity about 0.6%. The strain-rate predictions of the present model are very accurate for the stationary creep.

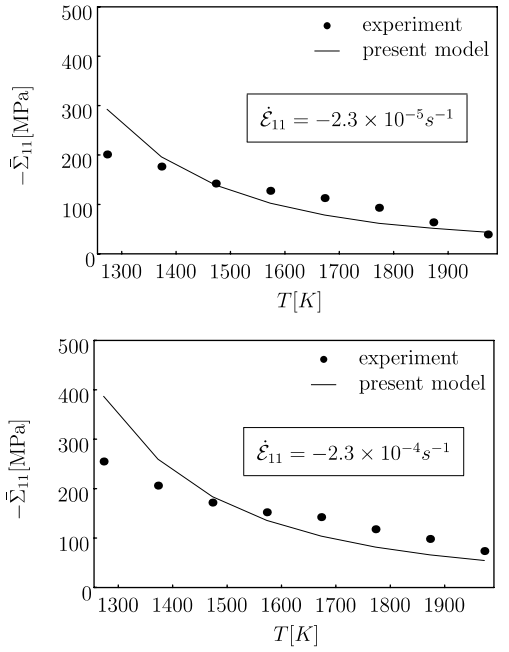

Fig. 4. Macroscopic ultimate steady stress for various temperatures during uniaxial compressive tests at different prescribed strain-rates: comparison between experimental data of Guerin (1975) and numerical simulations.

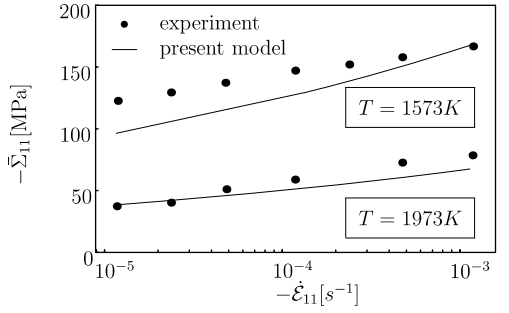

Fig. 5. Macroscopic ultimate steady stress for prescribed strain-rate during uniaxial compressive tests for various prescribed temperatures: comparison between experimental data of Guerin (1975) and numerical simulations.

3.3.2. Densification by mechanical loading

During compressive creeping tests, the densification by mechanical loading predicted by the present model is compared to the experimental data of Sladkoff et al. (2000), where the density of the nuclear pellet was measured before and after the test, and for nuclear pellets presenting various grain sizes (from 8.7 μm to 18.6 μm). The results are presented in Table 4 for a strain of approximately −3.22%. The model gives a very good estimate of

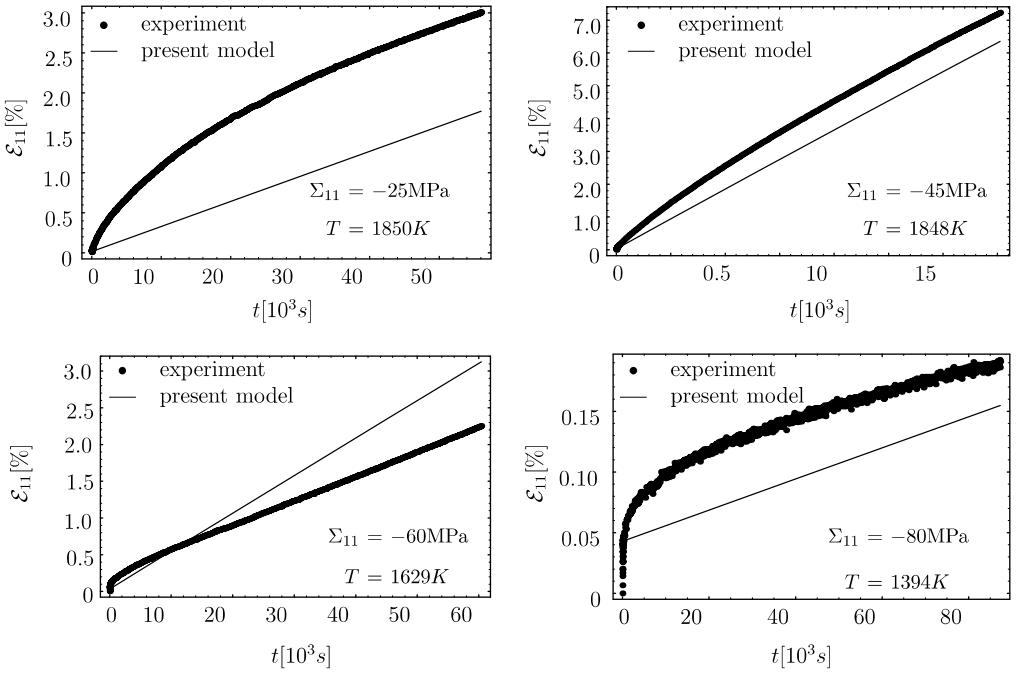

Fig. 6. Evolution of uniaxial strain with time during compressive creeping tests: comparison between experimental data of Sladkoff et al. (2000) and numerical simulations with the present model.

Table 4
Relative densification by mechanical loading during compressive tests: comparison between numerical simulation with the proposed model and experimental data of Sladkoff et al. (2000)

Numerical simulation with present model	Experimental results
$\simeq$0.14%	$\simeq$0.12%

this evolution of microstructure (densification) by mechanical loading.

In Fig. 7, the densification by mechanical loading predicted by the proposed model is compared to the experimental data of Paraschiv et al. (2002), where the evolution of the fuel density was measured at prescribed hydrostatic pressure and prescribed temperature during 280 h. Two temperature levels are studied: 1973 K and 2073 K; and the hydrostatic pressure varies from zero to 100 MPa. The initial porosity of the nuclear pellet is about 1.82% and the grain size is 8.2 μm. Comparison is plotted for the final density ($t = 280$ h).

3.3.3. Sensibility of the model to the grain size

In this section, a comparison of the sensitivity of the model to the grain size against results obtained during compressive tests at prescribed strain-rate ($\dot{\mathscr{E}}_{11} \simeq -2.5 \times 10^{-5}\ \mathrm{s}^{-1}$) (Sladkoff et al., 2000) is

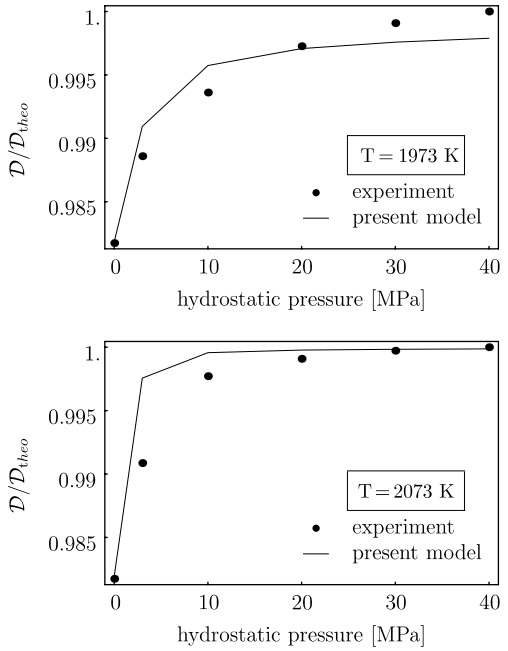

Fig. 7. Density of the nuclear fuel to theoretical density of UO_2 versus hydrostatic pressure after 280 h of constant hydrostatic loads at different prescribed temperatures: comparison between numerical simulations and experimental data of Paraschiv et al. (2002).

Table 5
Sample data form Sladkoff et al. (2000) for densification experiments

Grain size [μm]	Temperature [K]	Initial porosity [%]
4.5	1731	2.97
8.7	1738	4.71
11	1735	1.59
18.6	1740	3.94
20	1738	1.19
26	1741	1.02

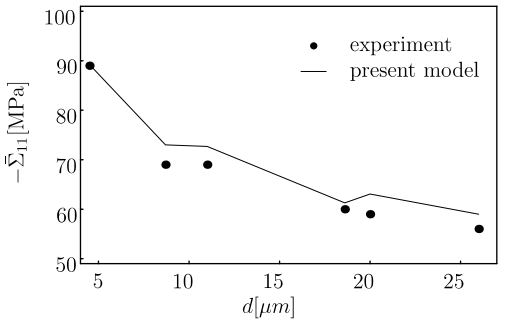

Fig. 8. Sensibility to grain size during compressive tests at prescribed velocity: comparison between ultimate steady stress predicted by the present model and experimentally measured.

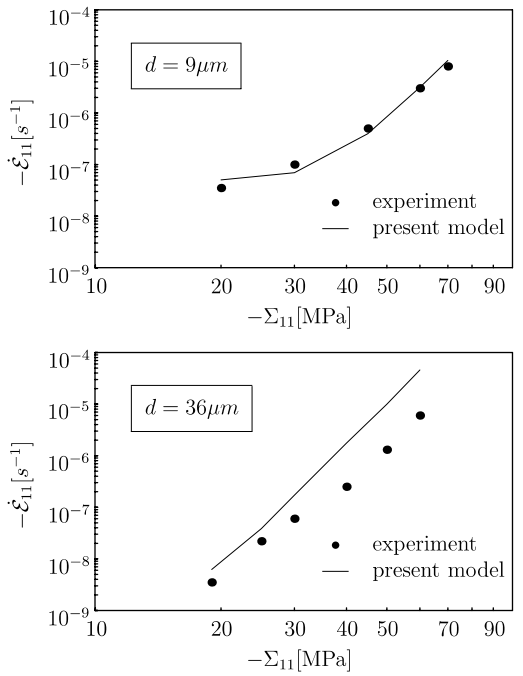

Fig. 9. Sensitivity to grain size during creep compressive tests: comparison between stationary strain-rate predicted by the present model and experimentally measured by Dherbey et al. (2002).

made. The studied cases are described in Table 5, and the comparison of experimental data and numerical results predicted by the present model is plotted in Fig. 8.

An other accurate sensitivity of the model to the grain size is plotted Fig. 9. The present model is compared to creeping compressive test data of Dherbey et al. (2002) performed at $T = 1738$ K and for $2.19\% \leqslant f \leqslant 2.70\%$. It should be underlined, as noticed by Dherbey et al. (2002), that the first regime is not visible for the $d = 36$ μm grain-sized pellets. This particular behavior is predicted by the present model.

4. Conclusion

An overall constitutive law for nonlinear viscous porous ceramics at high temperature involving two different Newtonian creeps at the microscale has been proposed. This model was identified and validated for the particular case of non-irradiated UO_2 nuclear fuel.

The proposed model was established by coupling, at the macroscale, two so-called hollow sphere models related to each microscopic creeping mechanism in presence of porosities (Michel and Suquet, 1992). Since microscopic creeping mechanisms are temperature-activated and take place for different ranges of temperature and stress, the effects of temperature were incorporated both on each sphere model and on the coupling function. This model could be summarized in the following way.

Two nonlinear viscous strain-rate potentials are considered at the microscale ($i = 1, 2$):

$$\psi_i(\sigma) = \frac{\sigma_{0_i}\dot{\bar{\varepsilon}}_{0_i}}{n_i+1}\left(\frac{\sigma_{\mathrm{eq}}}{\sigma_{0_i}}\right)^{n_i+1} d^{m_i}\mathrm{e}^{-\frac{Q_i}{RT}}. \tag{33}$$

Involving porosity effects, two quadratic strain-rate potentials are obtained at the macroscale ($i = 1, 2$):

$$\Psi_i(\Sigma, f) = \frac{\sigma_{0_i}\dot{\bar{\varepsilon}}_{0_i}}{n_i+1}\left[A(f)\left(\frac{3}{2}\frac{\Sigma_{\mathrm{m}}}{\sigma_{0_i}}\right)^2 + B(f)\left(\frac{\Sigma_{\mathrm{eq}}}{\sigma_{0_i}}\right)^2\right]^{\frac{n_i+1}{2}} d^{m_i}\mathrm{e}^{-\frac{Q_i}{RT}}, \tag{34}$$

where the "sphere model" terminology consists for $A(f)$ in the exact solution of an hollow sphere under hydrostatic loading, and for $B(f)$ in the rigorous nonlinear bound (see, e.g., Ponte Castañeda, 1991 or Talbot and Willis, 1992). A simple macroscopic coupling of both creeping mechanisms was proposed:

$$\Psi = (1-\theta)\Psi_1 + \theta\Psi_2, \tag{35}$$

where the coupling function θ depends on the temperature and on the stress (scattering-creep acts for lower temperatures and smaller stresses than dislocation-creep). The evolution of porosity was approximated by:

$$\dot{f} = (1-f)\mathrm{Tr}(\dot{\mathscr{E}}_{\mathrm{vp}}) = \frac{\partial \Psi}{\partial \Sigma_{\mathrm{m}}}. \tag{36}$$

This final model was coupled with the overall elastic behavior, assuming the additivity of macroscopic strains. A numerical semi-implicit solving scheme was proposed.

Microscopic mechanical parameters were taken equal to their theoretical estimates for the first creeping mechanism, and were identified on compressive creeping tests for the second creeping mechanism. The coupling function was identified on (Frost and Ashby, 1982) diagrams.

The obtained model was very accurately validated on compressive tests at various temperatures and at various prescribed strain-rates. This validation shows that the sensitivity to loading, temperature, and grain size is well taken into account, and that the volume change due to porosity evolution under mechanical loading (so-called swelling under tension and densification under compression) are conveniently predicted.

It should be noticed that the present model is the first model devoted to the stationary creep of nuclear ceramics based upon a micromechanical approach and exhibiting clearly the dependence of the UO_2 nuclear fuel to its microstructure and to elementary mechanisms acting in the UO_2 matrix.

Acknowledgments

The present study was supported by the Commissariat à l'Energie Atomique within the Pellet-Cladding Interaction program. The authors are indebted to Dr. P. Suquet and Dr. J.C. Michel for fruitful conversations and useful suggestions. Discussions with authors of (Sladkoff et al., 2000) including experiment data base are grateful acknowledged.

References

Armstrong, W., Irvine, W., 1963. Creep deformation of non-stoichiometric uranium dioxide. Journal of Nuclear Materials 9, 121–127.

Berg, C., 1970. Plastic dilatation and void interaction. In: Kaninen, M., Adler, W., Rosenfield, A., Jaffe, R. (Eds.), Inelastic Behavior of Solids. McGraw Hill, pp. 171–210.

Bohaboy, P., Asamoto, R., Conti, A., 1969. Compressive creep characteristics of stoichiometric uranium dioxide. GEAP-10054, General Electric Company, Sunnyvale.

Budiansky, B., Hutchinson, J., Slutsky, S., 1982. Void growth and collapse in viscous solids. In: Hopkins, H., Sewell, M. (Eds.), Mechanics of Solids, the Rodney Hill 60th Anniversary Volume. Pergamon Press, Oxford, pp. 607–652.

Burton, B., Reynolds, G., Barnes, J., 1973. The influence of grain size on the creep of uranium dioxide. Journal of Material Science 8, 1960–1964.

Chaboche, J.-L., Suquet, P., Beson, J., 2001. Endommagement et changement d'échelle. In: Bornert, M., Bretheau, T., Gilormini, P. (Eds.), Homogénéisation en mécanique des matériaux, vol. 2. Hermes Science, pp. 91–146 (Chapter 3).

Chung, T., Davies, T., 1979. The low-stress creep of fine-grain uranium dioxide. Acta Metallurgica 27, 627–635.

Cocks, A., 1989. Inelastic deformation of porous materials. Journal of the Mechanics and Physics of Solids 37, 693–715.

Dherbey, F., Louchet, F., Mocellin, A., Leclercq, S., 2002. Elevated temperature creep of polycrystalline uranium dioxide: from microscopic mechanisms to macroscopic behaviour. Acta Materialia 50, 1495–1505.

Duva, J., Hutchinson, J., 1984. Constitutive potentials for dilutely voided nonlinear materials. Mechanics of Materials 3, 41–54.

Frost, H., Ashby, M., 1982. Oxides with Fluorite Structure UO_2 and ThO_2. Pergamon Press, Oxford, p. 93.

Gatt, J.-M., Monerie, Y., Laux, D., Baron, D., 2005. Elastic behavior of porous ceramics: application to nuclear fuel materials. Journal of Nuclear Materials 336, 145–155.

Guerin, Y., 1975. Etude par compression à hautes températures de la déformation plastique du bioxyde d'uranium polycristallin. Journal of Nuclear Materials 56, 61–75.

Javed, N., 1975. Thermodynamics of Nuclear Materials. IAEA, Vienna.

Knorr, D., Cannon, R., Coble, R., 1989. An analysis of diffusion and diffusional creep in stoichiometric and hyperstoichiometric uranium dioxide. Acta Metallurgica 37, 2103–2123.

Leblond, J.-B., Perrin, G., 1992. Un modèle de comportement pour les matériaux viscoplastiques poreux. Comptes Rendus de l'Academie des Sciences Serie IIb (314), 987–993.

Leclercq, S., 1998. Modelling of the fuel mechanical behavior: from creep laws to internal variable models. Nuclear Engineering and Design 185, 221–228.

Martin, D., 1989. The elastic constants of polycrystalline UO_2 and (U,Pu) mixed oxides: a review and recommendations. High Temperatures–High Pressures 21, 13–24.

Michel, J.-C., 1994. A self-consistent estimate of the overall behavior of viscous and porous materials. Comptes Rendus de l'Academie des Sciences Serie IIb (319), 1439–1446.

Michel, J.-C., Suquet, P., 1992. The constitutive law of nonlinear viscous and porous materials. Journal of the Mechanics and Physics of Solids 40, 783–812.

Millet, C., Piconi, C., 1983. Fluage en pile de l'oxyde mixte UO_2–PuO_2. Journal of Nuclear Materials 116, 195–211.

Milton, G., 2002. The Theory of Composites. Cambridge University Press.

Nogita, K., Une, K., 1995. Irradiation-induced recrystallization in high burnup UO_2 fuel. Journal of Nuclear Materials 226, 302–310.

Olevsky, E., Skorohod, V., 1988. Some questions of sintering kinetics under external forces influence. In: Technological and

Design Plasticity of Porous Materials. IPMS NAS, Ukraine, p. 97.
Paraschiv, M., Paraschiv, A., Grecu, V., 2002. On the nuclear oxide fuel densification, swelling and thermal re-sintering. Journal of Nuclear Materials 302, 109–124.
Ponte Castañeda, P., 1991. The effective mechanical properties of nonlinear isotropic composites. Journal of the Mechanics and Physics of Solids 39, 45–71.
Ponte Castañeda, P., Willis, J., 1988. On the overall properties of nonlinearly viscous composites. Proceedings of the Royal Society of London Series A-Mathematical Physical and Engineering Sciences 416, 217–244.
Seltzer, M., Perrin, J., Clauer, A., Wilcox, B., 1971. A review of creep behavior of ceramic nuclear fuels. Reactor Technology 14, 99–135.
Shima, S., Oyane, M., 1976. Plasticity theory for porous metals. International Journal of Mechanical Science 18, 285–291.
Sladkoff, M., Huet, F., Mocellin, A., 2000. Uniaxial compressive tests on non irradiated UO_2 nuclear pellet, personal communication.
Sofronis, P., McMeeking, R., 1992. Creep in power-law material containing spherical voids. Journal of Applied Mechanics 59, S88–S95.
Suquet, P., 1982. Plasticité et homogénéisation. Thèse de Doctorat d'Etat, Université Pierre et Marie Curie, Paris 6.
Suquet, P., 1992. On bounds for the overall potential of power-law materials containing voids with arbitrary shape. Mechanical Research Communication 19, 51–58.
Talbot, D., Willis, J., 1992. Some explicit bounds for the overall behavior of nonlinear composites. International Journal of Solids and Structures 29, 1981–1987.
Wang, J., 2000. An investigation of the deformation mechanism in grain size-sensitive Newtonian creep. Acta Materialia 48, 1517–1531.
Wang, J., Nieh, T., 1996. A new interpretation of the mechanisms in Newtonian creep of uranium dioxides. Journal of Nuclear Materials 228, 141–147.
Zaoui, A., 2001. Changement d'échelle: motivation et méthodologie. In: Bornert, M., Bretheau, T., Gilormini, P. (Eds.), Homogénéisation en mécanique des matériaux, vol. 1. Hermes Science, pp. 19–40 (Chapter 1).